

High-bone-mass-producing mutations in the Wnt signaling pathway result in distinct skeletal phenotypes

Paul J. Niziolek^a, Takeisha L. Farmer^b, Yajun Cui^c, Charles H. Turner^d,
Matthew L. Warman^{e,f}, Alexander G. Robling^{b,d,*}

^a Weldon School of Biomedical Engineering, Purdue University, West Lafayette, IN, USA

^b Department of Anatomy & Cell Biology, Indiana University School of Medicine, Indianapolis, IN, USA

^c Department of Genetics, Case Western Reserve University School of Medicine, Cleveland, OH, USA

^d Department of Biomedical Engineering, Indiana University-Purdue University at Indianapolis, Indianapolis, IN, USA

^e Department of Orthopaedic Surgery, Children's Hospital, Boston, MA, USA

^f Howard Hughes Medical Institute, Department of Genetics, Harvard Medical School, Boston, MA, USA

ARTICLE INFO

Article history:

Received 13 May 2011

Revised 18 July 2011

Accepted 21 July 2011

Available online xxxx

Edited by: Robert Recker

Keywords:

Wnt

High bone mass

Lrp5

Sclerostin

Sost

ABSTRACT

Mutations among genes that participate in the canonical Wnt signaling pathway can lead to drastically different skeletal phenotypes, ranging from severe osteoporosis to severe osteosclerosis. Many high-bone-mass (HBM) causing mutations that occur in the LRP5 gene appear to impart the HBM phenotype, in part, by increasing resistance to soluble Wnt signaling inhibitors, including sclerostin. Sost loss-of-function mutant mice (Sost knock-out) and Lrp5 gain-of-function mutant mice (Lrp5 HBM knock-in) have high bone mass. These mutants potentially would be predicted to be phenocopies of one another, because in both cases, the sclerostin–Lrp5 interaction is disrupted. We measured bone mass, size, geometry, architecture, and strength in bones from three different genetic mouse models (Sost knock-out, Lrp5 A214V knock-in, and Lrp5 G171V knock-in) of HBM. We found that all three mouse lines had significantly elevated bone mass in the appendicular skeleton and in the cranium. Sost mutants and Lrp5 A214V mutants were statistically indistinguishable from one another in most endpoints, whereas both were largely different from the Lrp5 G171V mutants. Lrp5 G171V mutants preferentially added bone endocortically, whereas Lrp5 A214V and Sost mutants preferentially added bone periosteally. Cranial thickness and cranial nerve openings were similarly altered in all three HBM models. We also assessed serum serotonin levels as a possible mechanism accounting for the observed changes in bone mass, but no differences in serum serotonin were found in any of the three HBM mouse lines. The skeletal dissimilarities of the Lrp5 G171V mutant to the other mutants suggest that other, non-sclerostin-associated mechanisms might account for the changes in bone mass resulting from this mutation.

© 2011 Elsevier Inc. All rights reserved.

Introduction

Around the turn of this century, it was discovered that Wnt signaling had important functions in the mammalian skeleton [1]. Gene mapping studies demonstrated that the autosomal recessive human disease Osteoporosis-Pseudoglioma syndrome (OPPG) was caused by loss-of-function mutations in a co-receptor for Wnt proteins, the LDL-receptor related protein 5 (LRP5) [2]. Patients with OPPG have bone mineral densities of more than 5 standard deviations below the mean and are prone to skeletal fracture and deformity. Shortly after the discovery of families harboring loss-of-function mutations in LRP5, other investigators identified a series of single amino acid

missense mutations in LRP5 in several families that segregated abnormally high bone mass (HBM) in an autosomal dominant manner [3–5]. Although these patients had phenotypes that were reminiscent of a disorder of impaired osteoclast function—osteopetrosis—their clinical course and radiographic findings were distinctly different. For example, the general shape of their skeleton was normal and they had increased rather than decreased bone strength that is commonly associated with osteopetrosis.

A similar high bone mass (HBM) phenotype has been reported among patients with mutations in the SOST gene, or in its distant regulatory elements, which are linked to the sclerosing bone disorders Sclerosteosis and van Buchem's disease [6–8]. Similar to the LRP5 HBM patients, individuals with SOST mutations exhibit very high bone mass in the appendicular and axial skeleton [9–11]. *In vitro*, the protein product of the SOST gene—sclerostin—has been shown to bind and inhibit wild-type LRP5, but not LRP5 variants that harbor HBM-causing mutations [12–15]. Thus the phenotypic similarity among

* Corresponding author at: Department of Anatomy & Cell Biology, Indiana University School of Medicine, 635 Barnhill Dr., MS 5035, Indianapolis, IN 46202, USA. Fax: +1 317 278 2040.

E-mail address: arobling@iupui.edu (A.G. Robling).

LRP5 HBM patients and sclerosteosis/van Buchem's patients might have a common etiology: extracellularly unencumbered LRP5 activation. Presumably, in one case, WNT/LRP5 signaling proceeds unrestrained because sclerostin is unable to bind LRP5 and inhibit its intracellular signaling; in the other case, WNT/LRP5 signaling proceeds unrestrained because sclerostin is unavailable (absent) to inhibit LRP5 signaling. Either case might have the same outcome on intracellular targets immediately downstream of the LRP5 receptor.

Orthologous mouse models of Wnt-associated HBM conditions found in humans offer the opportunity to study the cellular mechanisms and ramifications of altered *in vivo* Wnt signaling on bone metabolism in greater detail than can be done clinically. We recently reported an HBM phenotype in two engineered *Lrp5* mouse models, in which we knocked-in two known HBM-causing mutations—a glycine to valine substitution at amino acid 171 (G171V) and an alanine to valine substitution at amino acid 214 (A214V) [16]. These mice express normal (wild-type) levels of mutant *Lrp5* in a spatially and temporally normal profile, due to the activity of the endogenous *Lrp5* promoter inherent in the knock-in strategy. In the present communication, we more closely compare these two *Lrp5* HBM knock-in models with each other, and to a *Sost* loss-of-function mouse model (*Sost* knock-out) [17]. We hypothesized that the *Lrp5* HBM knock-ins would manifest a skeletal phenocopy of the *Sost* mutants because of the presumed lack of *Sost*-mediated inhibition in all three models. We measured (1) the size and geometry of cortical bone sections from three different long bones, (2) trabecular bone architecture in a long bone metaphysis, (3) mechanical properties of two long bones using two different testing conditions, (4) skull thickness and morphology, and (5) serum 5-HT (serotonin) levels, as a potential explanation for the observed differences in bone mass [18].

We found that all three mouse lines had significantly elevated bone mass in the appendicular skeleton and in the cranium. For most of the cortical bone measurements and mechanical properties, *Sost* mutants and *Lrp5* A214V mutants were statistically indistinguishable from one another, whereas both were largely different from the *Lrp5* G171V mutants. *Lrp5* G171V mutants tended to add bone endocortically, whereas *Lrp5* A214V and *Sost* mutants tended to add bone periosteally. Cranial thickness was similarly elevated and cranial nerve openings were similarly reduced in all three lines, regardless of the mutation. The HBM phenotype was not associated with changes in serum serotonin levels for any of the three lines. In summary, the *Lrp5* A214V and *Lrp5* G171V mutations, while both producing high bone mass, resulted in significantly different phenotypes. *Lrp5* A214V mutants were strikingly similar to *Sost* mutants in many outcomes, suggesting that the *Lrp5* A214V mutation might confer immunity to sclerostin-mediated inhibition of the receptor. The dissimilarity of the *Lrp5* G171V mutant to the other mutants suggests that other, non-sclerostin-associated mechanisms might account for the changes in bone mass resulting from this mutation.

Materials and methods

Animals

Forty eight male mice, divided into six groups, were used for the experiments ($n=8/\text{group}$). The mice used were engineered to harbor one of three different mutations in the Wnt signaling pathway, or were wild-type control for each mutation. The mutations comprised *Sost* knockout (*Sost*^{-/-}), the gain-of-function (high-bone-mass producing) G171V mutation knocked in to the *Lrp5* locus (*Lrp5*^{G171V/G171V}), or the gain-of-function (high-bone-mass producing) A214V mutation knocked in to the *Lrp5* locus (*Lrp5*^{A214V/A214V}). Generation of these mutant mice has been described previously [16,17]. Briefly, the *Sost*^{-/-} mice were engineered by replacing ~90% of the *Sost* coding sequence and all of the single intron, with a Neomycin-resistance cassette, via homologous recombination. The

Lrp5 knock-in mice were engineered by replacing a portion of intron 2 through a portion of intron 4 with targeting constructs that harbored either the G171V (equivalent to residue 170 in the mouse) or the A214V (equivalent to residue 213 in the mouse) within exon 3, using homologous recombination. The *Sost*^{-/-} mice (and *Sost* WT relatives) were on a mixed genetic background of 129/SvJ and Black Swiss, and both *Lrp5* knock-in mutants (and their WT relatives) were on a mixed genetic background of 129S1/SvIMJ and C57Bl/6J. The mice were housed in cages of 3–5 and were given standard mouse chow (Harlan Teklad 2018SX; 1% Ca; 0.65% P; 2.1 IU/g vitamin D₃) and water *ad libitum*. When the mice reached 17 wks of age, they were sacrificed by CO₂ inhalation. The long bones and skull were dissected and fixed in 10% neutral buffered formalin. All procedures were performed in accordance with the Institutional Animal Care and Use Committee (IACUC) guidelines.

Micro-computed tomography (μCT)

Dissected bone samples were scanned on a desktop μCT (μCT -20; Scanco Medical, Bassersdorf, Switzerland). At 9 μm resolution, a single, transverse, tomographic slice was taken through the midshaft femur (50% of total length), the proximal tibia (74% of total length measured from the distal end), the mid-diaphyseal tibia (57% of total length measured from the distal end), the distal ulna (32.5% of total length measured from the distal end), the midshaft ulna (50% total length) and the proximal ulna (64% of total length measured from the distal end). Distal femur trabecular bone was quantified by scanning three representative slices through the metaphysis (71%, 76%, and 82% of total length). A 1.5 mm segment of the calvarium was scanned in the coronal plane at 15 μm resolution, in the region encompassing foramen ovale.

The distal femur μCT slices were manually segmented to isolate the trabecular compartment. Using the Scanco analysis software, the following static morphometric properties were derived from the trabecular bone as previously described [19]: bone volume (BV/TV), trabecular number (Tb.N), trabecular separation (Tb.Sp), and trabecular thickness (Tb.Th). The remaining analyses were performed in ImageJ using the raw ISQ files from each scan. Long bone cross-sectional slices (femur, tibia, ulna) were analyzed for cortical area (CA; mm²), medullary area (MA; mm²), total area (TA; mm²), and the maximum and minimum second moments of area (I_{MAX} and I_{MIN}, respectively; mm⁴). Calvarial μCT stacks were measured for the area of the foramen ovale by modeling a trapezoid between each sequential slice containing a portion of the foramen (15 μm slice thickness \times average foramen diameter between each slice) and summing the areas over the length of the foramen. Skull thickness (parietal bone thickness in the ectocranial–endocranial dimension) was measured from a single calvarial slice, on the slice bearing the rostro-caudal center of foramen ovale. The thickness was measured at three standardized locations.

Biomechanical measurements of whole bone strength

Whole tibiae and ulnae were soaked in a room temperature saline bath for 3 h prior to mechanical testing. For the tibial three-point tests, each tibia was positioned posterior side down across the two lower supports (spaced 11 mm apart) of a three-point bending apparatus, mounted in a Bose Electroforce 3200 electromagnetic test machine, which has a force resolution of 0.001 N [20,21]. The tibiae were loaded to failure in monotonic compression using a crosshead speed of 0.2 mm/s, during which force and displacement measurements were collected every 0.01 s.

For ulnar axial testing, each ulna was mounted distal end down and posterior end up between two opposing cup-shaped platens of the same Bose system described above. The bone was fixed in place using a ~0.2 N static preload and kept hydrated via a saline bath

attached to the lower platen. The ulnas were loaded to failure in monotonic compression using a crosshead speed of 2 mm/s, during which force and displacement measurements were collected every 0.01 s. From the tibial and ulnar force versus displacement curves, ultimate force, yield force, stiffness, and energy to failure were calculated using standard equations [22].

Serum serotonin measurements

Serum samples were collected via tail bleeds 3 days prior to sacrifice. Tail blood was collected in 3 non-heparinized capillary tubes, allowed to clot for 30 min, and then separated via centrifugation. The serum fraction was removed and stored at -80°C until the day of analysis. Serum concentration of 5-HT (serotonin) was measured in duplicate by competitive ELISA (Fitzgerald Industries International) following the manufacturer's instructions.

Statistical methods

Each endpoint was analyzed for statistical significance using two-way Analysis of Variance (ANOVA), in which the locus (*Sost*, *Lrp5* 214, and *Lrp5* 171) and genotype (wild-type vs. mutant) were main effects. When a significant locus by genotype interaction was found, Fisher's PLSD post-hoc tests were conducted to determine differences among individual loci. All mutation effects were tested for significance using one-way ANOVA. For all tests, significance was taken at $p < 0.05$.

Results

Long bone size and geometry

Because loss-of-function mutations in the *Sost* gene and gain-of-function mutations in the *Lrp5* gene would be expected to have

similar effects on downstream Wnt signaling in bone cells (both are pro-canonical Wnt signaling), we compared the size and geometric properties of the long bones from *Sost* knock-out mice (*Sost*^{-/-}) with those of two *Lrp5* gain-of-function knock-in mice (*Lrp5*^{A214V/A214V} and *Lrp5*^{G171V/G171V}) to assess whether mutation at these loci would produce phenocopies of each other. As expected, all three mutants exhibited significantly increased cortical bone size (cortical area and total area) in the femur, tibia, and ulna, compared to their respective WT controls (Figs. 1–3 lower left panels, and Table 1). In addition, the minimum second moments of area (I_{MIN})—a geometric measurement of the bone's capacity to resist bending about its weakest plane—was also significantly increased in all three mutants. The maximum second moment area (I_{MAX}) was significantly increased in all cortical sites from all long bones studied in the *Sost* and *Lrp5* A214V mutants, but only half of the cortical sites studied yielded a significant increase in I_{MAX} among the *Lrp5* G171V mutants (Figs. 1–3 lower right panels, and Table 1).

Among the cortical bone size measurements that yielded a significant locus \times genotype interaction term (i.e., indicating that the mutation affected cortical bone size differently, depending on the locus), follow-up comparisons indicated that *Lrp5* A214V mutants and the *Lrp5* G171V mutants were consistently different from one another, whereas the *Sost* mutants were statistically indistinguishable from the *Lrp5* A214V mutants in a majority of the cortical measurements (Table 1).

Trabecular bone architecture

Because mutations in the Wnt pathway are known to affect trabecular bone properties, we also evaluated trabecular mass and architecture among the three mutant lines to assess whether the locus-associated differences observed in cortical properties extended to the trabecular envelope. All trabecular bone architectural properties evaluated were significantly enhanced in all three mutant mice,

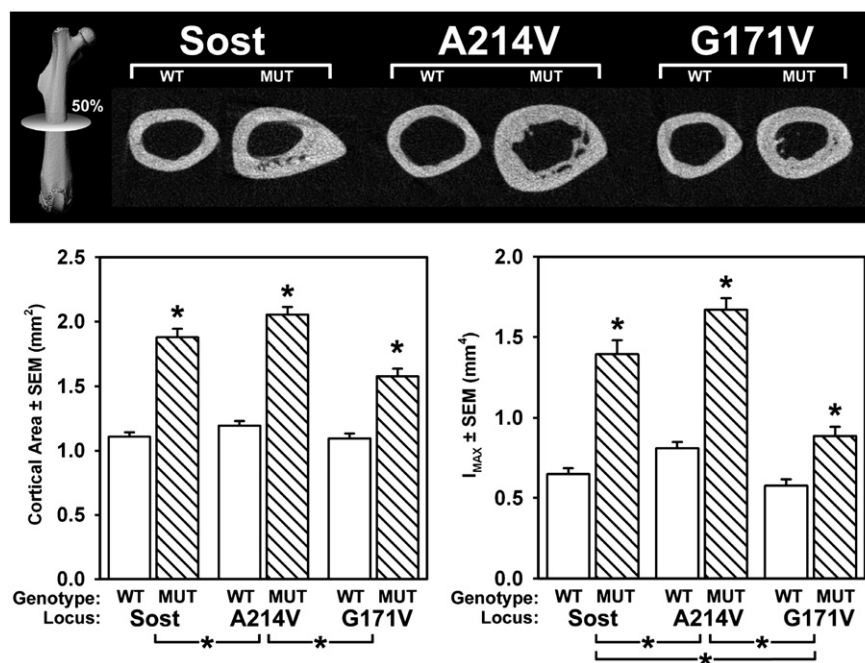


Fig. 1. (Top panel) A single μCT slice through the midshaft femur reveals a significant increase in cortical bone area (lower left panel) among mutant (MUT) mice, compared to their colony-matched wild type (WT) controls, in all three lines (*Sost*, *Lrp5* A214V, and *Lrp5* G171V). Two-way ANOVA on cortical area indicated a significant mutation effect (WT vs MUT), a significant locus effect (*Sost* vs A214V vs G171V), and a significant interaction between mutation and locus. Post-hoc tests revealed that the *Lrp5* A214V sections were significantly different from the remaining two mouse lines (indicated by brackets beneath the panel), suggesting that the mutation affected cortical area significantly more than in the *Sost* and *Lrp5* G171V mutants. Midshaft femur I_{MAX} (lower right panel), a measure of bone geometry, was also increased significantly by the mutation in all three mouse lines. Two-way ANOVA on I_{MAX} indicated a significant mutation effect (WT vs MUT), a significant locus effect (*Sost* vs A214V vs G171V), and a significant interaction between mutation and locus. All three mouse lines were significantly different from one another in the mutation-associated change in I_{MAX} (by brackets beneath the panel), with the A214V mutants exhibiting the greatest mutation-associated gain in I_{MAX} . An expanded set of midshaft femur cortical bone data is presented in Table 1. * indicates $p < 0.05$.

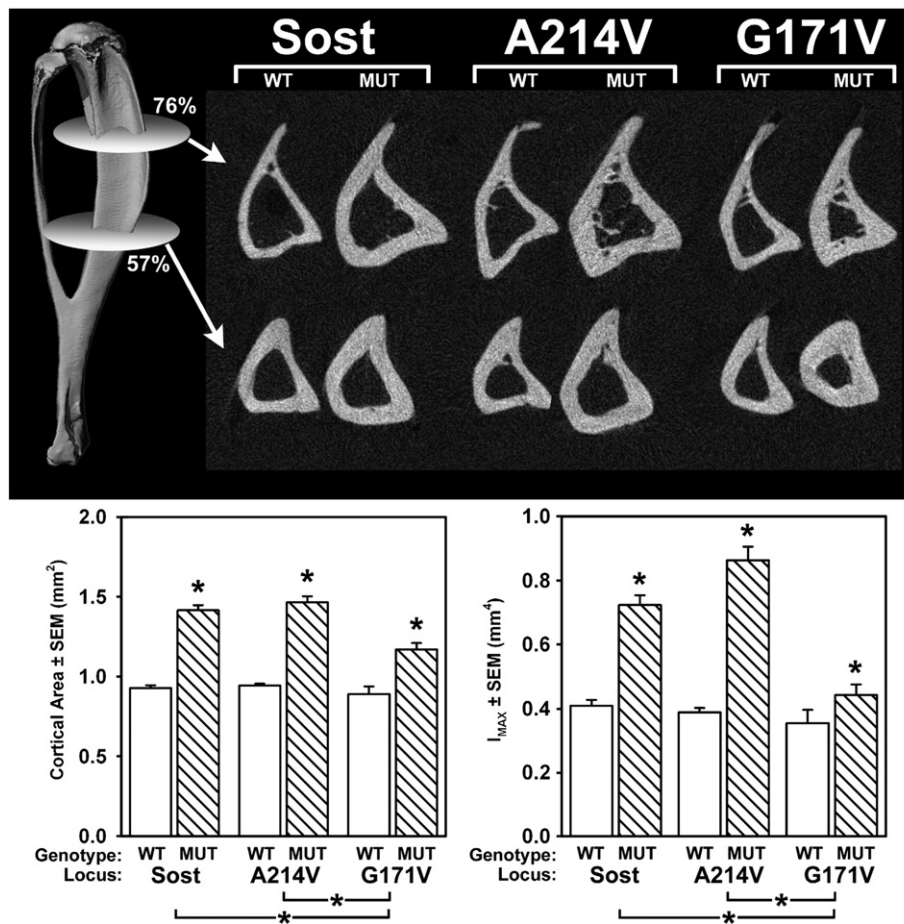


Fig. 2. (Top panel) A μ CT slice through the proximal tibia (76% of total length), and the slice near the mid-diaphyseal tibia (57%) reveal a significant increase in cortical bone area (lower left panel quantifies the 57% slice; the 76% slice is quantified in Table 1) among mutant (MUT) mice, compared to their colony-matched wild type (WT) controls, in all three lines (Sost, Lrp5 A214V, and Lrp5 G171V). Two-way ANOVA on cortical area indicated a significant mutation effect, a significant locus effect, and a significant interaction between mutation and locus. Post-hoc tests revealed that the Lrp5 G171V sections were significantly different from the remaining two mouse lines (indicated by brackets beneath the panel), suggesting that the mutation affected cortical area more severely in the Sost and Lrp5 A214V mutants, compared to the Lrp5 G171V mutants. Mid-diaphyseal tibia I_{MAX} (lower right panel), a measure of bone geometry, was also increased significantly by the mutation in all three mouse lines. Two-way ANOVA on I_{MAX} indicated a significant mutation effect (WT vs MUT), a significant locus effect (Sost vs A214V vs G171V), and a significant interaction between mutation and locus. Post-hoc tests revealed that the Lrp5 G171V sections were significantly different from the remaining two mouse lines (indicated by brackets beneath the panel), suggesting that the mutation affected cortical geometry more severely in the Sost and Lrp5 A214V mutants, compared to the Lrp5 G171V mutants. An expanded set of tibia cortical bone data is presented in Table 1. * indicates $p < 0.05$.

compared to their respective WT controls (Fig. 4 and Table 1). Both BV/TV and Tb.N exhibited significant locus \times genotype interaction terms, indicating that the mutation affects trabecular bone mass and structure differently, depending on the locus. Follow-up tests on these two parameters indicated that two Lrp5 mutants were significantly different from the Sost mutants. Tb.Th and Tb.Sp, while elevated in all three mutants, were not differentially affected by the genetic locus.

Cranial morphology and mass

Both Sost loss-of-function and Lrp5 gain-of-function mutations have been associated with increases in skull thickness and morphology among patient populations. We measured skull thickness along a standardized location in the parietal bone among the three mutant mouse lines to determine if these mice model the human skull phenotypes, and to ascertain whether the locus-associated differences observed in the appendicular skeleton were manifest in the skull. Parietal thickness was increased 60–80% in mutant mice, compared to their respective WT controls (Fig. 5). The locus \times genotype interaction term for parietal thickness did not reach statistical significance ($p = 0.068$), so pairwise differences among groups were not pursued.

In light of the reports in the literature describing cranial foramen stenosis (and associated nerve function impairment) among many sclerosteosis and van Buchem's disease patients, we also probed the skulls for the area of foramen ovale, an opening in the basicranium that transmits the V₃ division of the trigeminal nerve and a few smaller structures (lesser petrosal nerve, accessory meningeal artery). All three mutant mice exhibited smaller foramina than their respective WT controls, but statistical significance was reached only for the Sost and Lrp5 G171V mice (Fig. 6). Of the two main effects (locus and genotype), and their interaction, only the genotype yielded a significant result, indicating that the foramen size was reduced equally among mutants in the three mouse lines.

Whole bone biomechanical properties

We measured mechanical properties of whole tibiae and ulnae to ascertain whether the differences observed in bone mass and shape were accompanied by similar changes in bone strength. Whole tibiae from Sost and Lrp5 A214V, but not G171V, mutants exhibited significantly increased properties in three point bending (Fig. 7 and Table 2), with the exception of energy to failure among the Lrp5 A214V mice. Tibiae from Lrp5 G171V mutants failed to reach a

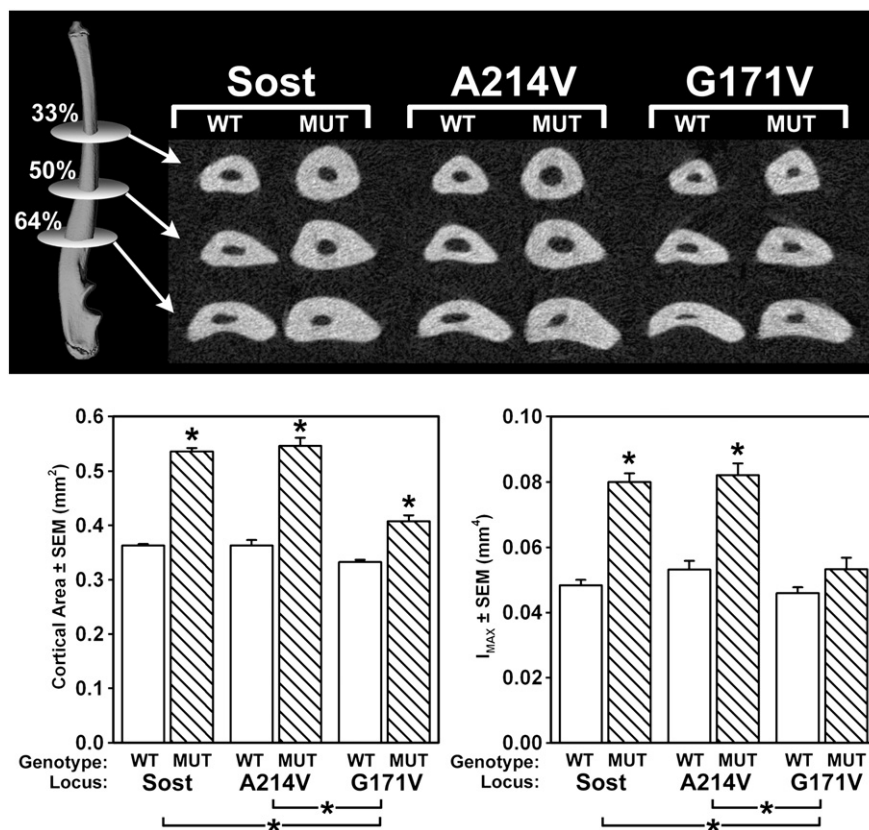


Fig. 3. (Top panel) A μ CT slice through the distal ulna (33% of total length), the midshaft ulna (50% of total length), and the proximal ulna (64% of total length), reveal a significant increase in cortical bone area (lower left panel quantifies the midshaft slice; the 33% and 64% slices are quantified in Table 1) among mutant (MUT) mice, compared to their colony-matched wild type (WT) controls, in all three lines (Sost, Lrp5 A214V, and Lrp5 G171V). Two-way ANOVA on cortical area indicated a significant mutation effect, a significant locus effect, and a significant interaction between mutation and locus. Like the mid-diaphyseal tibia, post-hoc tests revealed that the Lrp5 G171V ulnar sections were significantly different from the remaining two mouse lines (indicated by brackets beneath the panel), suggesting that the mutation affected cortical area more severely in the Sost and Lrp5 A214V mutants, compared to the Lrp5 G171V mutants. Midshaft ulnar I_{MAX} (lower right panel), a measure of bone geometry, was also increased significantly by the mutation in Sost and Lrp5 A214V mutants, but not in the Lrp5 G171V mutants. Two-way ANOVA on I_{MAX} indicated a significant mutation effect, a significant locus effect, and a significant interaction between mutation and locus. Post-hoc tests revealed that the Lrp5 G171V sections were significantly different from the remaining two mouse lines (indicated by brackets beneath the panel), suggesting that the mutation affected cortical geometry more severely in the Sost and Lrp5 A214V mutants, compared to the Lrp5 G171V mutants. An expanded set of ulnar cortical bone data is presented in Table 1. * indicates $p < 0.05$.

significant increase in any of the properties measured. No significant locus \times genotype interactions were found for the tibial tests.

Whole ulnae from the same mice were tested in monotonic compression in the axial direction, and all three lines exhibited significantly greater ultimate force (Fig. 7) and stiffness (Table 2) among mutants. Energy to failure and yield force were significantly enhanced in Sost and Lrp5 A214V mutants, but not in Lrp5 G171V mutants, compared to WT controls (Table 2). All mechanical parameters measured in the ulna yielded a significant locus \times genotype interaction term, indicating that the mutation affected ulnar bone strength differently, depending on the locus. Follow-up comparisons indicated that Sost mutants and the Lrp5 A214V mutants were statistically similar, and both were consistently different from the Lrp5 G171V mutants. Ulnae from all three genotypes exhibited fracture at approximately the same point ($\sim 1/3$ rd of the distance from the distal end) along the ulnar shaft.

Serum serotonin levels

In order to explore the possibility that serum serotonin measurements might be associated with the high bone mass phenotype in the Sost and Lrp5 mutants, we measured serotonin in the serum of these mice via sandwich ELISA (Fig. 8). Serotonin levels were not different in any of the three mutants, compared to their respective WT controls. No significant locus or genotype effects were found for these measurements.

Discussion

The main objective in our study was to evaluate the phenotypic similarity among high-bone-mass mice harboring mutations in the Wnt signaling pathway that all presumably affect the same molecular interaction (sclerostin-mediated inhibition of Lrp5). We found that the Lrp5 A214V mutants and the Sost mutants were not significantly different from one another at a majority of cortical bone sites. This result is surprising; we expected Sost mutant mice to exhibit the greatest increase in bone mass and strength. Sost is known to bind and inhibit both Lrp5 and Lrp6, both of which have been shown to regulate bone mass. In the Sost mutants, both Lrp5 and Lrp6 were relieved from sclerostin-mediated inhibition, but among the Lrp5 A214V mutants, even if the mutation conferred resistance to sclerostin-mediated inhibition in the Lrp5 receptor, the Lrp6 receptor would still be vulnerable to sclerostin-mediated inhibition in these mice. Thus it is unclear why the A214V mutation generated equally robust, and in some cases, more robust cortical phenotypes (e.g., proximal tibia) than the Sost mutation.

Perhaps more perplexing is the obvious difference in bone properties between the two Lrp5 mutants. Although both Lrp5 mutants exhibited significantly increased bone mass, in nearly every cortical measurement, we found that the A214V mutants were significantly larger (i.e., more bone, greater periosteal dimensions, improved geometric properties) than the G171V mutants. Conversely, the G171V mutants exhibited significantly reduced medullary areas (MA) in their

Table 1
μCT-derived cortical and trabecular bone properties in Sost knock-out, Lrp5 A214V knock-in, and Lrp5 G171V knock-in mice.

	Sost		Lrp5 A214V		Lrp5 G171V	
	WT	MUT	WT	MUT	WT	MUT
Cortical bone properties						
Midshaft femur						
I_{MAX} (mm ⁴) ^{A,B,C}	0.64 ± 0.04	1.37 ± 0.08 ^{*1,2}	0.80 ± 0.04	1.64 ± 0.07 ^{*1}	0.57 ± 0.04	0.87 ± 0.06 [*]
I_{MIN} (mm ⁴) ^{A,B,C}	0.33 ± 0.03	0.58 ± 0.05 ^{*2}	0.48 ± 0.03	0.96 ± 0.05 ^{*1}	0.34 ± 0.03	0.51 ± 0.04 [*]
Total area (mm ²) ^{A,B,C}	1.98 ± 0.04	2.57 ± 0.08 ^{*2}	2.38 ± 0.05	3.17 ± 0.07 ^{*1}	1.94 ± 0.05	2.26 ± 0.06 [*]
Medullary area (mm ²) ^{A,B}	0.88 ± 0.03	0.69 ± 0.04 [*]	1.19 ± 0.04	1.11 ± 0.04	0.85 ± 0.04	0.68 ± 0.04 [*]
Cortical area (mm ²) ^{A,B,C}	1.11 ± 0.04	1.88 ± 0.07 ^{*2}	1.19 ± 0.03	2.05 ± 0.06 ^{*1}	1.09 ± 0.04	1.58 ± 0.06 [*]
Mid-tibia (57%)						
I_{MAX} (mm ⁴) ^{A,B,C}	0.40 ± 0.02	0.71 ± 0.03 ^{*1}	0.38 ± 0.01	0.85 ± 0.04 ^{*1}	0.35 ± 0.04	0.43 ± 0.03 [*]
I_{MIN} (mm ⁴) ^{A,B,C}	0.20 ± 0.01	0.39 ± 0.03 ^{*1}	0.21 ± 0.01	0.46 ± 0.02 ^{*1}	0.16 ± 0.02	0.24 ± 0.01 [*]
Total area (mm ²) ^{A,B,C}	1.40 ± 0.03	1.90 ± 0.05 ^{*1}	1.36 ± 0.02	2.07 ± 0.05 ^{*1}	1.21 ± 0.07	1.45 ± 0.04 [*]
Medullary area (mm ²) ^{A,B,C}	0.48 ± 0.02	0.48 ± 0.02	0.42 ± 0.02	0.60 ± 0.03 ^{*1}	0.33 ± 0.03	0.28 ± 0.02
Cortical area (mm ²) ^{A,B,C}	0.93 ± 0.02	1.41 ± 0.03 ^{*1}	0.94 ± 0.01	1.46 ± 0.04 ^{*1}	0.89 ± 0.05	1.17 ± 0.04 [*]
Proximal tibia (74%)						
I_{MAX} (mm ⁴) ^{A,B,C}	0.68 ± 0.02	1.08 ± 0.04 ^{*1,2}	0.89 ± 0.04	1.52 ± 0.11 ^{*1}	0.71 ± 0.06	0.81 ± 0.04
I_{MIN} (mm ⁴) ^{A,B,C}	0.26 ± 0.02	0.55 ± 0.04 ^{*1,2}	0.30 ± 0.02	0.74 ± 0.03 ^{*1}	0.22 ± 0.02	0.35 ± 0.02 [*]
Total area (mm ²) ^{A,B,C}	1.72 ± 0.05	2.22 ± 0.06 ^{*1,2}	1.78 ± 0.04	2.59 ± 0.07 ^{*1}	1.43 ± 0.08	1.72 ± 0.05 [*]
Medullary area (mm ²) ^{A,C}	0.79 ± 0.03	0.68 ± 0.04 ^{*1}	0.70 ± 0.03	0.86 ± 0.03 ^{*1}	0.46 ± 0.03	0.38 ± 0.03
Cortical area (mm ²) ^{A,B,C}	0.93 ± 0.03	1.53 ± 0.04 ^{*1,2}	1.07 ± 0.02	1.73 ± 0.06 ^{*1}	0.97 ± 0.05	1.33 ± 0.06 [*]
Distal ulna (33%)						
I_{MAX} (mm ⁴) ^{A,B,C}	0.025 ± 0.001	0.042 ± 0.002 ^{*1}	0.021 ± 0.001	0.043 ± 0.003 ^{*1}	0.015 ± 0.000	0.023 ± 0.002 [*]
I_{MIN} (mm ⁴) ^{A,B,C}	0.010 ± 0.001	0.029 ± 0.001 ^{*1}	0.011 ± 0.001	0.037 ± 0.003 ^{*1}	0.008 ± 0.000	0.013 ± 0.001 [*]
Total area (mm ²) ^{A,B,C}	0.33 ± 0.01	0.49 ± 0.01 ^{*1}	0.32 ± 0.01	0.53 ± 0.02 ^{*1}	0.27 ± 0.00	0.34 ± 0.01 [*]
Medullary area (mm ²) ^{A,B,C}	0.032 ± 0.003	0.040 ± 0.004 ^{1,2}	0.035 ± 0.004	0.065 ± 0.005 ^{*1}	0.017 ± 0.002	0.012 ± 0.002
Cortical area (mm ²) ^{A,B,C}	0.30 ± 0.006	0.45 ± 0.008 ^{*1}	0.28 ± 0.006	0.46 ± 0.017 ^{*1}	0.25 ± 0.004	0.33 ± 0.012 [*]
Midshaft ulna						
I_{MAX} (mm ⁴) ^{A,B,C}	0.048 ± 0.002	0.080 ± 0.003 ^{*1}	0.053 ± 0.003	0.082 ± 0.004 ^{*1}	0.046 ± 0.002	0.053 ± 0.004
I_{MIN} (mm ⁴) ^{A,B,C}	0.011 ± 0.001	0.029 ± 0.001 ^{*1,2}	0.014 ± 0.001	0.035 ± 0.002 ^{*1}	0.008 ± 0.000	0.014 ± 0.001 [*]
Total area (mm ²) ^{A,B,C}	0.39 ± 0.00	0.57 ± 0.01 ^{*1}	0.43 ± 0.02	0.60 ± 0.02 ^{*1}	0.35 ± 0.01	0.42 ± 0.01 [*]
Medullary area (mm ²) ^A	0.029 ± 0.001	0.033 ± 0.002	0.063 ± 0.006	0.057 ± 0.002	0.018 ± 0.004	0.017 ± 0.002
Cortical area (mm ²) ^{A,B,C}	0.36 ± 0.00	0.54 ± 0.01 ^{*1}	0.36 ± 0.01	0.55 ± 0.01 ^{*1}	0.33 ± 0.00	0.41 ± 0.01
Proximal ulna (64%)						
I_{MAX} (mm ⁴) ^{A,B,C}	0.098 ± 0.003	0.145 ± 0.005 ^{*1}	0.105 ± 0.004	0.155 ± 0.008 ^{*1}	0.104 ± 0.003	0.106 ± 0.006
I_{MIN} (mm ⁴) ^{A,B,C}	0.015 ± 0.001	0.030 ± 0.001 ^{*1}	0.016 ± 0.001	0.034 ± 0.002 ^{*1}	0.013 ± 0.001	0.018 ± 0.001 [*]
Total area (mm ²) ^{A,B,C}	0.48 ± 0.01	0.66 ± 0.01 ^{*1}	0.49 ± 0.01	0.69 ± 0.02 ^{*1}	0.45 ± 0.01	0.53 ± 0.01 [*]
Medullary area (mm ²) ^{A,B,C}	0.040 ± 0.004	0.022 ± 0.002 ^{*1}	0.036 ± 0.002	0.022 ± 0.003 ^{*1}	0.015 ± 0.006	0.014 ± 0.003
Cortical area (mm ²) ^{A,B,C}	0.440 ± 0.007	0.640 ± 0.008 ^{*1}	0.460 ± 0.010	0.670 ± 0.020 ^{*1}	0.440 ± 0.008	0.520 ± 0.015 [*]
Trabecular bone properties						
Distal femur						
Tb.N (#/mm ²) ^{A,B,C}	2.09 ± 0.10	4.91 ± 0.11 ^{*1,2}	2.58 ± 0.12	5.94 ± 0.11 [*]	2.08 ± 0.08	7.32 ± 0.09 [*]
Tb.Th (mm) ^B	28.5 ± 8.9	59.3 ± 11.1 [*]	37.4 ± 10.4	60.5 ± 10.3 [*]	30.8 ± 9.5	58.7 ± 11.1 [*]
Tb.Sp (mm) ^B	881.1 ± 96.9	156.9 ± 24.3 [*]	623.6 ± 87.0	112.3 ± 23.0 [*]	805.2 ± 75.9	79.4 ± 16.8 [*]

* Significant difference between mutant and wild-type control.

^A Significant locus effect (Sost, 171, 214) yielded from 2-way ANOVA.^B Significant mutation effect (wild-type vs mutation) yielded from 2-way ANOVA.^C Significant locus by mutation interaction yielded from 2-way ANOVA.¹ Locus is significantly different from G171V locus (based on post hoc test following a significant locus by mutation interaction).² Locus is significantly different from A214V locus (based on post hoc test following a significant locus by mutation interaction).

long bones, whereas the A214V mutants usually exhibited either no change or increased MA. Moreover, the G171V mutants exhibited the greatest increase in trabecular bone mass and architecture, though it was not statistically different from the Lrp5 A214V mutants (Fig. 4). In light of these observations, there appears to be a fundamental difference in the way that these two mutations affect bone size and shape, perhaps affecting Wnt signaling differently. This result is curious given that both A214V and G171V mutations are in the same exon, and both reside in the same pocket near the surface of the first β-propeller within the EGF-like domain. Although both mutations confer resistance to sclerostin- and Dkk1-mediated inhibition *in vitro*, functional differences between these two mutations have been noted. For example, the G171V mutation has increased responsiveness to a Wnt1 signal in an *in vitro* assay, whereas the A214V mutation does not confer increased Wnt1 responsiveness [23]. Additionally, when overexpressed, the G171V mutation has been found to traffic poorly to the cell surface [24]. This has led some investigators to postulate an intracellular, autocrine signaling mechanism for this mutational

effect, though the defective trafficking function might be an artifact of overexpression and not a primary defect *in vivo*. The A214V mutation appears to traffic through the cells as efficiently as the wild-type receptor [23].

The HBM-causing mutations have been reported to confer resistance not only to sclerostin-mediated inhibition, but also to Dkk1-mediated inhibition. Dkk1 and sclerostin bind to different β-propeller domains of the Lrp5 receptor, and their inhibitory action is additive, not synergistic [25]. Furthermore, Dkk1 is a much stronger binding partner to WT Lrp5 than is sclerostin, and it is able to displace pre-bound sclerostin from the receptor [25]. In the Lrp5 mutants we studied, Dkk1 would presumably have had no effect on Lrp5 signaling, whereas in the Sost mutants, Dkk1 should be fully capable of inhibiting Wnt/Lrp5 signaling. The observation that Sost mutants have such high bone mass suggests little compensation by the other Wnt signaling inhibitors, including Dkk1, to keep bone formation in check in the absence of sclerostin. Conversely, removal of sclerostin from the system (e.g., Sost mutants) would not “free up” any new

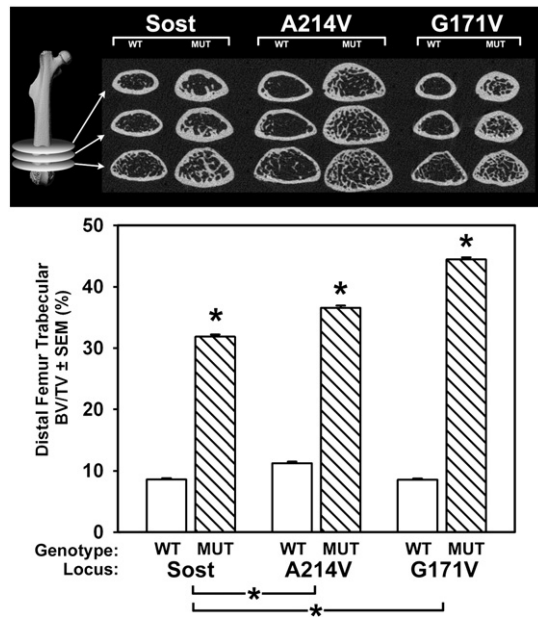


Fig. 4. (Top panel) Three standardized μ CT slices through the distal femur (71%, 76%, and 82% of total length) reveal a significant increase in trabecular bone mass and architecture in all three mutant (MUT) lines, compared to their colony-matched wild type (WT) controls. (Lower panel) Bone volume fraction (BV/TV) was significantly increased in all three lines. Two-way ANOVA on BV/TV indicated a significant mutation effect, a significant locus effect, and a significant interaction between mutation and locus. Post-hoc tests revealed that the Lrp5 G171V and A214V metaphyseal compartment was populated with more trabecular bone than in the Sost mutants, but no difference between Lrp5 mutants was detected (indicated by brackets beneath the panel). An expanded set of trabecular bone data is presented in Table 1. * indicates $p < 0.05$.

binding sites for Dkk1 since this molecule does not compete for the same binding site on Lrp5, nor does it interact with sclerostin. Recently, it was reported that sclerostin requires a co-factor, identified

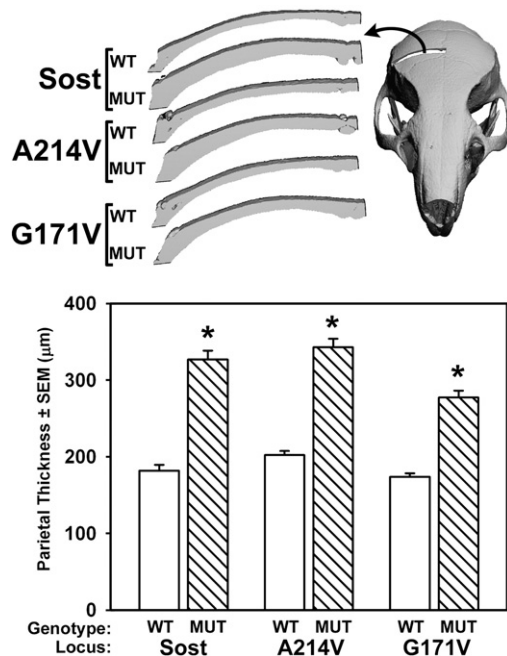


Fig. 5. (Top panel) Representative μ CT reconstructions of 40 slices taken from the central portion of the parietal bone reveal increased skull thickness in all three mutant lines (MUT), compared to WT controls. Two-way ANOVA on skull thickness indicated a significant mutation effect, a significant locus effect, but no significant interaction between mutation and locus ($p = 0.065$), indicating that the mutation affected skull thickness equally in all three lines. * indicates $p < 0.05$.

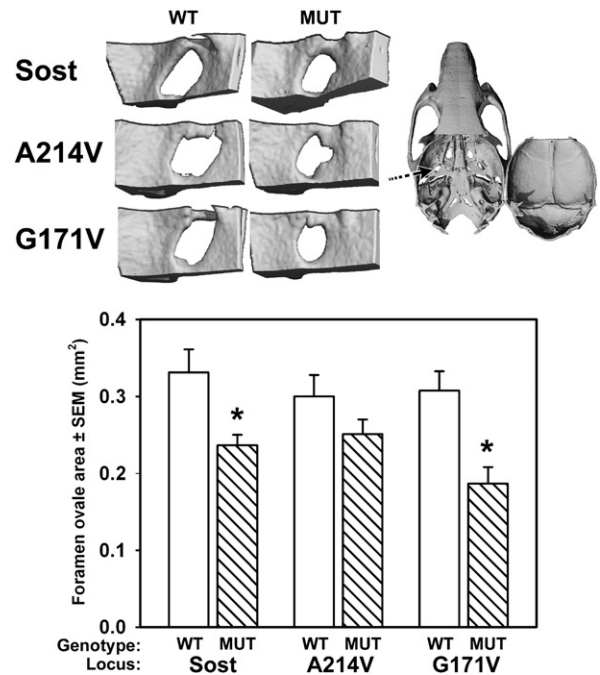


Fig. 6. (Top panel) Representative μ CT reconstructions of ~ 70 slices taken from a portion of the ethmoid bone, revealing an interior view of foramen ovale. Note the decrease in size of the foramen in all three mutants. The reduction failed to reach significance in the Lrp5 A214V mutants. * indicates $p < 0.05$.

as Lrp4, to exert its inhibitory effect on Lrp5/6 action in bone cells [26]. Lrp4 deletion would be expected to result in high bone mass, but Lrp4-null mice (Lrp4^{-/-}) do not survive gestation and preclude such an evaluation [27]. Mice harboring hypomorphic alleles for Lrp4 survive to adulthood, but the osteopenia, growth retardation, and skeletal malformations are manifest [28], highlighting Lrp4's more complex role in development, and in other tissues, than has been attributed to Sost.

We previously reported mechanical properties from femoral three point bending tests in the Lrp5 HBM knock-in mice. In those experiments, we found significant increases in mechanical properties of the femoral shaft among both A214V and G171V mutants [16]. In the present study, we conducted similarly designed tests on the tibia, and extended our analyses to include an axial compression test (ulna). Although we found significant increases in mechanical properties in the tibiae from the Lrp5 A214V mutants, confirming our earlier reports in the femur, we failed to find a significant increase in bone strength among G171V mutant tibiae. We did, however, find significantly increased mechanical properties (ultimate force, stiffness) among all three mutant lines, including the G171V mutants, in the ulnar axial compression tests. The increased cortical area (largely from addition of bone to the endocortical surface) in the Lrp5 G171V mutants resulted in increased strength in the axial tests, which are more influenced by cross sectional area than are pure bending tests.

A transgenic model for the Lrp5 G171V mutation has been previously reported. In that model, human Lrp5 cDNA, containing the G171V mutation, is driven by the 3.6 kb fragment of the rat type I collagen promoter [29]. Mice harboring the transgene (Col3.6::G171V) had significantly greater bone mass, which could mostly be accounted for by increased periosteal expansion, and they also exhibited significantly greater bone strength than their non-transgenic littermates [30]. In our knock-in model of the equivalent mouse mutation, we found increased bone mass, but not because of periosteal expansion. Furthermore, the lack of periosteal expansion in our G171V knock-ins resulted in largely unaffected bending properties, when compared to wild-type controls (Table 2). These discrepancies between models

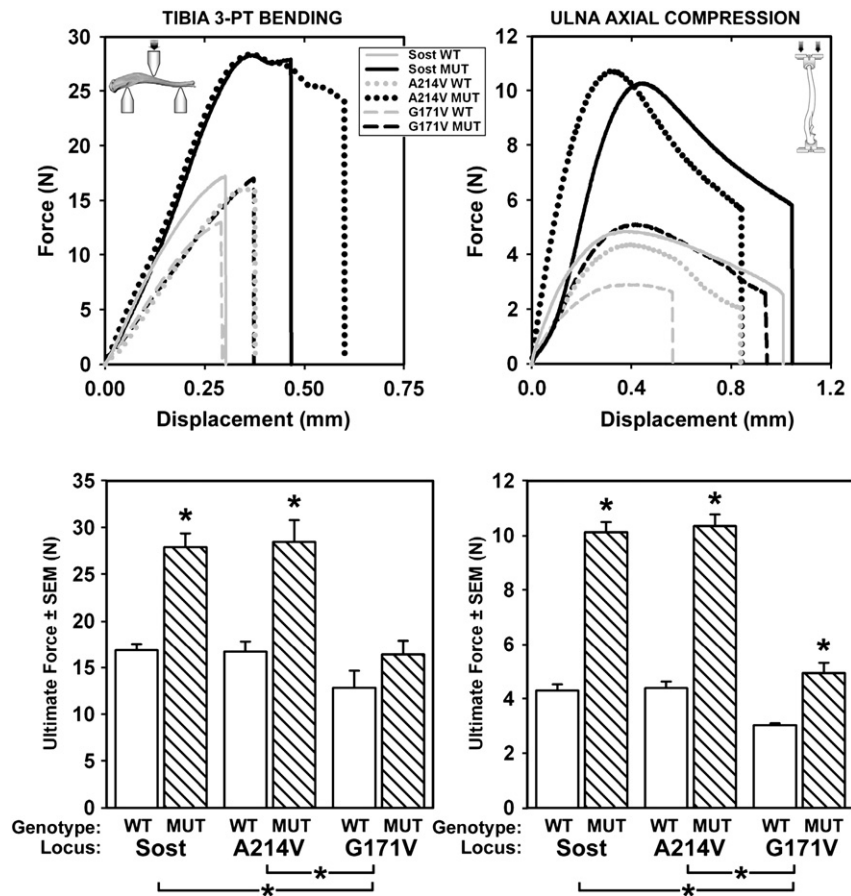


Fig. 7. (Top panel) Representative force vs. displacement curves from 3-point bending tests on the tibia (upper left) and axial compression tests on the ulna (upper right panel). Note the large and significant increase in tibial bone strength among the Sost and Lrp5 A214V mutants, but not in the Lrp5 G171V mutants. The lack of effect in the Lrp5 G171V mutants can be verified by inspecting the mid-diaphyseal sections presented in Fig. 2 (upper panel), which show modest gains in total bone size in these mice. Ulnar bone strength was significantly increased in all three mutants (lower right panel), but post-hoc tests revealed that the increased ultimate force was significantly greater in the Sost and Lrp5 A214V mutants, compared to the changes induced in the Lrp5 G171V mutants (indicated by brackets beneath the panel). An expanded set of mechanical properties data is presented in Table 2. * indicates $p < 0.05$.

are likely the result of different mouse engineering strategies, which affect the number of copies of the receptor expressed, and the timing and tissue-specificity of receptor expression. It will be interesting to learn whether the G171V knock-in allele confers increased sensitivity to mechanical loading, as has been reported for the G171V transgenic mouse model.

Patients with SOST and SOST-associated mutations (e.g., sclerosteosis, van Buchem's disease) frequently present clinically with impaired

hearing, balance, vision, taste perception, and facial muscle palsy, all of which can be attributed to nerve impingement where the cranial nerves supplying these functions course through the skull [31–35]. In the Sost mutant mice, we were able to confirm a stenotic phenotype at foramen ovale. If the reduced area of this foramen is representative of the other cranial foramina and fissures in these mice, then the Sost mutant mice represent a useful model for therapies aimed at nerve function restoration in the patient population. Surprisingly, we also

Table 2

Whole bone mechanical properties derived from three point bending tests of the tibia and axial compression tests of the ulna.

	Sost		Lrp5 A214V		Lrp5 G171V	
	WT	MUT	WT	MUT	WT	MUT
Tibia 3-point bending						
Energy to failure (mJ) ^A	4.26 ± 0.66	6.72 ± 0.76*	5.12 ± 0.83	7.36 ± 1.55	2.78 ± 0.47	3.16 ± 0.36
Stiffness (N/mm) ^{A,B}	59.9 ± 3.6	101.1 ± 7.5*	62.0 ± 4.0	112.6 ± 13.0*	46.7 ± 7.1	65.2 ± 5.1
Yield force (N) ^{A,B}	13.8 ± 0.92	21.7 ± 1.69*	15.0 ± 1.26	21.8 ± 2.60*	9.3 ± 0.74	14.8 ± 1.14
Ulna axial compression						
Energy to failure (mJ) ^{A,B,C}	3.68 ± 0.29	6.73 ± 0.38* ¹	2.95 ± 0.21	6.75 ± 0.39* ¹	1.76 ± 0.25	2.92 ± 0.45
Stiffness (N/mm) ^{A,B,C}	14.7 ± 1.74	35.3 ± 1.64* ¹	16.2 ± 1.13	40.3 ± 2.26* ¹	10.7 ± 0.32	21.2 ± 1.95*
Yield force (N) ^{A,B,C}	2.15 ± 0.72	7.28 ± 1.36* ¹	1.91 ± 0.70	8.88 ± 0.49* ¹	1.68 ± 0.61	2.80 ± 0.57

* Significant difference between mutant and wild-type control.

^A Significant locus effect (Sost, G171V, A214V) yielded from 2-way ANOVA.

^B Significant mutation effect (wild-type vs mutation) yielded from 2-way ANOVA.

^C Significant locus by mutation interaction yielded from 2-way ANOVA.

¹ Locus is significantly different from G171V locus (based on post hoc test following a significant locus by mutation interaction).

² Locus is significantly different from A214V locus (based on post hoc test following a significant locus by mutation interaction).

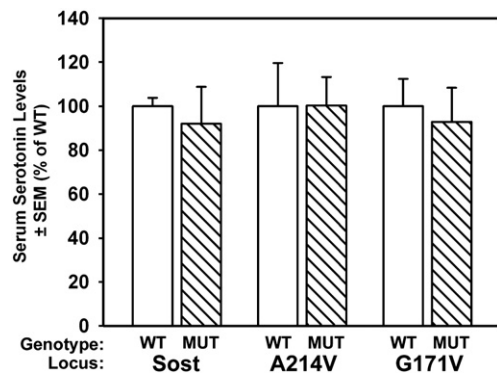


Fig. 8. Serum serotonin measurements were performed on blood samples taken from the study mice several days before sacrifice (~17 wks). Serotonin was not significantly different in any of the mutant (MUT) mouse lines, when compared to wild type (WT) controls.

confirmed a stenotic foramen phenotype among the *Lrp5* mutants, despite a lack of reported impairment in cranial nerve function among the LRP5 HBM patient population. If the patient population is orthologous to the mouse models we report here, there is some indication that these patients might suffer many of the motor and sensory functional deficiencies associated with cranial nerve impingement. This possibility will need to await further clinical data for verification. Perhaps more serious than the loss of sensory function among the sclerosteosis/van Buchem's patients is the life-threatening increases intracranial pressure that develops around the brain as a result of overgrowth of the endocranial table of the cranial vault bones [32]. Not surprisingly, we were able to confirm a large increase in skull thickness in the *Sost* mutants, but also in both *Lrp5* mutants.

We were unable to detect any significant changes in serum serotonin levels in the mutant mice when compared to WT controls. In a previous report, using numerous mouse models, we investigated whether *Lrp5* controls serotonin synthesis in the intestine, and whether serotonin blood levels affect bone mass [16]. We found that activation and inactivation of *Lrp5* in bone, but not in intestine, alter bone mass, and that no association between *Lrp5* genotype and blood serotonin levels, or between serotonin level and bone mass, could be detected. The results in the present study confirm our earlier results, and expand our scope to include the *Sost* mutants, further suggesting that the Wnt-related HBM-causing mutations function independently of serum serotonin levels.

In summary, we found that three mutant mice that presumably nullify the sclerostin–*Lrp5* interaction have significantly different phenotypes. *Lrp5* HBM mutant mice that harbor a single missense mutation at different base pairs within exon 3 exhibit considerable morphological difference in the post-cranial skeleton. It is unlikely that these differences can be explained by differences in receptor expression levels, location, or timing, because they share a common, endogenous promoter. *Sost* mutations confer increased bone properties that are morphologically very similar to *Lrp5* A214V mutant mice. Genetic crosses that challenge the *Lrp5* HBM knock-in lines with enhanced and dysregulated expression of putatively ineffective soluble inhibitors (e.g., *Dkk1* and/or *Sost* overexpresser lines) would add considerable insight into the mechanisms by which the HBM-causing mutations in *Lrp5* produce increased bone mass.

Acknowledgments

This work was supported by NIH grant AR53237 (to AGR), the Howard Hughes Medical Institute (to MLW), and NIH grant AR046530 (to CHT). The *Sost* mutant mice were kindly provided by Chris Paszty and Amgen, Inc.

References

- Johnson ML, Harnish K, Nusse R, Van Hul W. LRP5 and Wnt signaling: a union made for bone. *J Bone Miner Res* 2004;19:1749–57.
- Gong Y, Slee RB, Fukai N, Rawadi G, Roman-Roman S, Reginato AM, et al. LDL receptor-related protein 5 (LRP5) affects bone accrual and eye development. *Cell* 2001;107:513–23.
- Ferrari SL, Deutsch S, Choudhury U, Chevalley T, Bonjour JP, Dermizakis ET, et al. Polymorphisms in the low-density lipoprotein receptor-related protein 5 (LRP5) gene are associated with variation in vertebral bone mass, vertebral bone size, and stature in whites. *Am J Hum Genet* 2004;74:866–75.
- Little RD, Carulli JP, Del Mastro RG, Dupuis J, Osborne M, Folz C, et al. A mutation in the LDL receptor-related protein 5 gene results in the autosomal dominant high-bone-mass trait. *Am J Hum Genet* 2002;70:11–9.
- Van Wesenbeeck L, Cleiren E, Gram J, Beals RK, Benichou O, Scopelliti D, et al. Six novel missense mutations in the LDL receptor-related protein 5 (LRP5) gene in different conditions with an increased bone density. *Am J Hum Genet* 2003;72:763–71.
- Balemans W, Ebeling M, Patel N, Van Hul E, Olson P, Dioszegi M, et al. Increased bone density in sclerosteosis is due to the deficiency of a novel secreted protein (SOST). *Hum Mol Genet* 2001;10:537–43.
- Balemans W, Patel N, Ebeling M, Van Hul E, Wuyts W, Lacza C, et al. Identification of a 52 kb deletion downstream of the *SOST* gene in patients with van Buchem disease. *J Med Genet* 2002;39:91–7.
- Staebling-Hampton K, Proll S, Paepfer BW, Zhao L, Charnley P, Brown A, et al. A 52-kb deletion in the *SOST*-*MEOX1* intergenic region on 17q12–q21 is associated with van Buchem disease in the Dutch population. *Am J Med Genet* 2002;110:144–52.
- Beighton P, Cremin BJ, Hamersma H. The radiology of sclerosteosis. *Br J Radiol* 1976;49:934–9.
- Beighton P, Durr L, Hamersma H. The clinical features of sclerosteosis. A review of the manifestations in twenty-five affected individuals. *Ann Intern Med* 1976;84:393–7.
- Gardner JC, van Bezooijen RL, Mervis B, Hamdy NA, Lowik CW, Hamersma H, et al. Bone mineral density in sclerosteosis; affected individuals and gene carriers. *J Clin Endocrinol Metab* 2005;90:6392–5.
- Li X, Zhang Y, Kang H, Liu W, Liu P, Zhang J, et al. Sclerostin binds to LRP5/6 and antagonizes canonical Wnt signaling. *J Biol Chem* 2005;280:19883–7.
- Semenov M, Tamai K, He X. SOST is a ligand for LRP5/LRP6 and a Wnt signaling inhibitor. *J Biol Chem* 2005;280:26770–5.
- Semenov MV, He X. LRP5 mutations linked to high bone mass diseases cause reduced LRP5 binding and inhibition by SOST. *J Biol Chem* 2006;281:38276–84.
- Ellies DL, Viviano B, McCarthy J, Rey JP, Itasaki N, Saunders S, et al. Bone density ligand, sclerostin, directly interacts with LRP5 but not LRP5G171V to modulate Wnt activity. *J Bone Miner Res* 2006;21:1738–49.
- Cui Y, Niziolek PJ, MacDonald BT, Zylstra CR, Alenina N, Robinson DR, et al. *Lrp5* functions in bone to regulate bone mass. *Nat Med* 2011;17:684–91.
- Li X, Ominsky MS, Niu QT, Sun N, Daugherty B, D'Agostin D, et al. Targeted deletion of the sclerostin gene in mice results in increased bone formation and bone strength. *J Bone Miner Res* 2008;23:860–9.
- Yadav VK, Ryu JH, Suda N, Tanaka KF, Gingrich JA, Schutz G, et al. *Lrp5* controls bone formation by inhibiting serotonin synthesis in the duodenum. *Cell* 2008;135:825–37.
- Sawakami K, Robling AG, Ai M, Pitner ND, Liu D, Warden SJ, et al. The Wnt co-receptor LRP5 is essential for skeletal mechanotransduction but not for the anabolic bone response to parathyroid hormone treatment. *J Biol Chem* 2006;281:23698–711.
- Robling AG, Hinant FM, Burr DB, Turner CH. Improved bone structure and strength after long-term mechanical loading is greatest if loading is separated into short bouts. *J Bone Miner Res* 2002;17:1545–54.
- Schriefer JL, Robling AG, Warden SJ, Fournier AJ, Mason JJ, Turner CH. A comparison of mechanical properties derived from multiple skeletal sites in mice. *J Biomech* 2005;38:467–75.
- Turner CH, Burr DB. Basic biomechanical measurements of bone: a tutorial. *Bone* 1993;14:595–608.
- Ai M, Holmen SL, Van Hul W, Williams BO, Warman ML. Reduced affinity to and inhibition by DKK1 form a common mechanism by which high bone mass-associated missense mutations in LRP5 affect canonical Wnt signaling. *Mol Cell Biol* 2005;25:4946–55.
- Zhang Y, Wang Y, Li X, Zhang J, Mao J, Li Z, et al. The LRP5 high-bone-mass G171V mutation disrupts LRP5 interaction with Mesd. *Mol Cell Biol* 2004;24:4677–84.
- Balemans W, Piters E, Cleiren E, Ai M, Van Wesenbeeck L, Warman ML, et al. The binding between sclerostin and LRP5 is altered by DKK1 and by high-bone mass LRP5 mutations. *Calcif Tissue Int* 2008;82:445–53.
- Leupin O, Piters E, Halleux C, Hu S, Kramer I, Morvan F, et al. Bone overgrowth-associated mutations in LRP4 impair sclerostin-facilitator function. *J Biol Chem* 2011;286:19489–500.
- Weatherbee SD, Anderson KV, Niswander LA. LDL-receptor-related protein 4 is crucial for formation of the neuromuscular junction. *Development* 2006;133:4993–5000.
- Choi HY, Dieckmann M, Herz J, Niemeier A. *Lrp4*, a novel receptor for Dickkopf 1 and sclerostin, is expressed by osteoblasts and regulates bone growth and turnover in vivo. *PLoS One* 2009;4:e7930.
- Babij P, Zhao W, Small C, Kharode Y, Yaworsky PJ, Bouxsein ML, et al. High bone mass in mice expressing a mutant LRP5 gene. *J Bone Miner Res* 2003;18:960–74.

- [30] Akhter MP, Wells DJ, Short SJ, Cullen DM, Johnson ML, Haynatzki GR, et al. Bone biomechanical properties in LRP5 mutant mice. *Bone* 2004;35:162–9.
- [31] Beighton P, Hamersma H. Ophthalmological complications in the sclerosing bone dysplasias. *Ophthalmic Paediatr Genet* 1985;6:129–34.
- [32] Hamersma H, Gardner J, Beighton P. The natural history of sclerosteosis. *Clin Genet* 2003;63:192–7.
- [33] Hamersma H, Hofmeyr L. Too much bone: the middle ear in sclerosing bone dysplasias. *Adv Otorhinolaryngol* 2007;65:61–7.
- [34] Nager GT, Hamersma H. Sclerosteosis involving the temporal bone: histopathologic aspects. *Am J Otolaryngol* 1986;7:1–16.
- [35] Stephen LX, Hamersma H, Gardner J, Beighton P. Dental and oral manifestations of sclerosteosis. *Int Dent J* 2001;51:287–90.